JPET Fast Forward. Published on October 29, 2015 as DOI: 10.1124/jpet.115.226761
This article has not been copyedited and formatted. The final version may differ from this version.

METHYLMERCURY-DEPENDENT INCREASES IN FLUO4 FLUORESCENCE IN NEONATAL RAT CEREBELLAR SLICES DEPEND ON GRANULE CELL MIGRATIONAL STAGE AND $GABA_A$ RECEPTOR MODULATION

Aaron B. Bradford, Jayme D. Mancini and William D. Atchison

Department of Pharmacology and Toxicology[WDA]
Department of Biochemistry and Molecular Biology[AAB]
Center for Integrative Toxicology[AAB, WDA]
Neuroscience Program[JDM]
Michigan State University
East Lansing, MI, USA 48824-1317

JPET Fast Forward. Published on October 29, 2015 as DOI: 10.1124/jpet.115.226761
This article has not been copyedited and formatted. The final version may differ from this version.

RUNNING TITLE PAGE

Running Title: Cerebellar Granule Cells, $GABA_A$Rs & MeHg Ca^{2+} dysregulation *(59 spaces)*

Address all correspondence including reprint requests to:
Dr. William Atchison

Department of Pharmacology and Toxicology

Michigan State University

B-331 Life Science Building

1355 Bogue Street

East Lansing, MI 48824-1317

Phone: **(517) 353-4947**

Fax: **(517) 432-1341**

Emails: **atchiso1@msu.edu** (WDA, corresponding author)

aaronbbradford@gmail.com (ABB)

jaymemancini@hotmail.com (JDM)

DOCUMENT STATISTICS

Number of text pages: 22

Number of tables: 0

Number of Figures: 11

Number of references: 66

Number of words in Abstract: 250

Number of words in Introduction: 806

Number of words in Discussion: 1647

JPET Fast Forward. Published on October 29, 2015 as DOI: 10.1124/jpet.115.226761
This article has not been copyedited and formatted. The final version may differ from this version.

Non-standard abbreviations:

ACSF- artificial cerebrospinal fluid

CGC- cerebellar granule cell

EGL- external granule cell layer

ethD-1 ethidium homodimer-1

GABA- gamma amino butyric acid

$GABA_AR$- GABA A-type receptor

IGL- internal granule cell layer

Ca^{2+}_i- intracellular Ca^{2+}

MeHg- methylmercury

ML- molecular layer

NMDA- N-methyl-d-aspartate

NW- no wash

PC- Purkinje cells

VGCCs- voltage-gated Ca^{2+} channels

JPET Fast Forward. Published on October 29, 2015 as DOI: 10.1124/jpet.115.226761
This article has not been copyedited and formatted. The final version may differ from this version.

ABSTRACT

Methylmercury (MeHg) disrupts cerebellar function, especially during development. Cerebellar granule cell (CGC) cells, which are particularly susceptible to MeHg, but by unknown mechanisms, migrate during this process. Transient changes in intracellular Ca^{2+} (Ca^{2+}_i) are crucial to proper migration, and MeHg is well known to disrupt CGC Ca^{2+}_i regulation. Acutely prepared slices of neonatal rat cerebellum, in conjunction with confocal microscopy and fluo-4 epifluorescence were used to track changes induced by MeHg in CGC Ca^{2+}_i regulation in the external (EGL) and internal granule cell layers (IGL) as well as the molecular layer (ML). MeHg caused no cytotoxicity, but did cause a time-dependent increase in fluo-4 fluorescence that depended on the stage of granule cell development. CGCs in the EGL were most susceptible to MeHg-induced increases in fluo-4 fluorescence. MeHg increased fluorescence in CGC processes, but only diffusely; Purkinje cells rarely fluoresced in these slices. Neither muscimol nor bicuculline alone altered baseline fluo-4 fluorescence in any CGC layer, but each delayed the onset and reduced the magnitude of effect of MeHg on fluo-4 fluorescence in the EGL and ML. In the IGL, both muscimol and bicuculline delayed the onset of MeHg-induced increases in fluo-4 fluorescence, but didn't affect fluorescence magnitude. Thus acute exposure to MeHg causes developmental stage-dependent increases in Ca^{2+}_i in CGCs. Effects are most prominent in CGCs during development, or early stages of migration. $GABA_A$ receptors participate in an as yet unclear manner to MeHg-induced Ca^{2+}_i dysregulation of CGCs.

INTRODUCTION

Methylmercury (MeHg) is a widespread environmental neurotoxicant known to affect the cerebellum (Hunter and Russell, 1954, Takeuchi *et al*., 1962, Bakir *et al*., 1973). MeHg is especially toxic to cerebellar granule cells (CGCs), the smallest and most numerous neurons in the brain. CGCs die following both chronic and acute MeHg poisoning, whereas a higher percentage of neighboring Purkinje cells (PCs) survive, despite accumulating more MeHg than do CGCs (Hunter and Russell, 1954, Sakamoto *et al*., 1998, Edwards *et al*., 2005, Yuan and Atchison, 2007).

The developing cerebellum is especially sensitive to neurotoxicity induced by MeHg. Dysmorphogenesis, with loss of the characteristic "layering" of the cerebellar cortex occurs following *in utero* exposure of humans to MeHg (Philbert *et al.*, 2000, for review). Cerebellar architecture is critically dependent upon migration of CGCs and synaptogenesis. CGCs undergo a highly regimented and organized migration pattern in which their precursors divide and migrate from the external granule cell layer (EGL) along the processes of Bergmann glia, through the maturing PC dendrites in the molecular layer (ML) and mature in the internal granule layer (IGL) (Komuro and Rakic, 1998). They undergo distinct patterns of migration through the layers. Initially migration is tangential to the EGL, then radial through the ML and finally into the IGL (Komuro and Rakic, 1998). Human fetuses exposed to MeHg during CGC migration show the greatest susceptibility to toxicity (Amin-Zaki *et al*., 1974). Rats and mice are also susceptible to MeHg during a postnatal period of CGC migration, suggesting it is not the time before or after birth that determines susceptibility, but rather some mechanism involved in neuronal migration and survival (Rice and Barone, 2000, Sakamoto *et al.*, 2004).

CGC migration has been studied extensively in isolated acutely prepared slices (Komuro

JPET Fast Forward. Published on October 29, 2015 as DOI: 10.1124/jpet.115.226761
This article has not been copyedited and formatted. The final version may differ from this version.

and Rakic, 1995), as well as organotypic slice culture (Komuro and Rakic, 1995, Kunimoto and Suzuki, 1997, Mancini and Atchison, 2007). CGC migration depends on transient increases in intracellular calcium concentration ($[Ca^{2+}]_i$) (Komuro and Rakic, 1998; Komuro and Kamada, 2005), which, in turn, are modulated by N-type (Cav2.2) voltage-gated Ca^{2+} channels (VGCCs) (Komuro and Rakic, 1992), N-methyl-d-aspartate (NMDA) receptors (Komuro and Rakic, 1993), and intracellular signaling pathways (Komuro and Rakic, 1995; Komuro *et al.*, 2015). When those transient changes in $[Ca^{2+}]_i$ are disrupted, migration ceases (Kumada and Komuro, 2004). Thus interrupting the frequency, or timing of these $[Ca^{2+}]_i$ pulses would be expected to interrupt CGC migration, thereby impairing the ultimate development of cerebellar cortex layering.

One recurring observation of effects of MeHg on CGCs is that it disrupts regulation of $[Ca^{2+}]_i$ (Marty and Atchison, 1997; 1998; Limke and Atchison, 2002; Limke *et al.*, 2003; 2004, Yuan and Atchison, 2007). In cerebellar slices from mature rats, acute exposure to MeHg increases fluo-4 fluorescence and simultaneously stimulates, then inhibits release of both glutamate and GABA (Yuan and Atchison, 2007). In addition to its ability to interact with $GABA_A$Rs, MeHg also interacts with several types of VGCC, including Cav2.2 (Shafer and Atchison, 1991, Sirois and Atchison, 2000, Peng *et al*., 2002, Hajela *et al*., 2003). The lasting effects of MeHg on CGC $[Ca^{2+}]_i$ result from complex interactions with both intracellular Ca^{2+} pools in the smooth endoplasmic reticulum and mitochondria, as well as with these voltage-gated Ca^{2+} channels. Each of these sources of $[Ca^{2+}]_i$ are vital to CGC migration. Thus disruption of their normal function could have dire consequences for establishing and sustaining the pulses of $[Ca^{2+}]_i$ shown to be essential for proper migration of CGCs. Continuous MeHg treatment delays CGC migration in all layers, suggesting that disruption of Ca^{2+} oscillations occurs (Mancini *et al*., 2010).

Among the pathways that control activation of Cav2.2 channels in developing CGCs, $GABA_A$Rs play an underappreciated role. Whereas in mature CGCs, $GABA_A$Rs are inhibitory, their activation in immature CGCs leads to Cl^- efflux, and thus inward current (Owens *et al.*,1996), thereby depolarizing the CGC membrane (Takayama and Inoue, 2004a,b). This occurs due to the altered expression of the cation transporters KCC1 and NKCC1, which are abundantly expressed in immature neurons, whereas KCC2 is not (Mikawa *et al.*, 2002; Yamada *et al.,* 2004; Takayama and Inoue, 2006). The resulting shift in Cl^- gradient results in a $GABA_A$R-mediated depolarization which could rapidly activate proximal, voltage-gated channels.

The pattern of $GABA_A$R subunit expression also differs markedly between migrating and post-migratory CGCs (Takayama and Inoue, 2004a,b). This is especially true for the α subunit which contains the ligand binding sites, and markedly influences both the GABA sensitivity as well as the kinetic properties of the receptor. Mature CGCs express a myriad of $GABA_A$R subunits including the α1, α6, several β subunits, both long and short splice variants of γ3, and most uniquely, the δ subunit (Laurie *et al.*, 1992). Conversely, in the migrating and premigratory state CGCs express the α2 subunit (Takayama and Inoue, 2004a,b). MeHg has complex interactions with CGC $GABA_A$Rs. In mature CGCs in slice it initially increases $GABA_A$R current before ultimately blocking current flow (Yuan and Atchison, 2007). In neonatal granule cells in culture, MeHg at low concentrations causes a time-dependent block of GABA-mediated current (Herden *et al.*, 2008). However the effects of MeHg on $GABA_A$Rs in migrating, immature neurons have yet to be described.

We sought to test the hypothesis that CGCs at different stages of development react differentially to MeHg by investigating the acute actions of MeHg on developing CGCs. Slices

JPET Fast Forward. Published on October 29, 2015 as DOI: 10.1124/jpet.115.226761
This article has not been copyedited and formatted. The final version may differ from this version.

of brain maintained in oxygenated artificial cerebrospinal fluid (ACSF) permit rapid and controlled treatment of cells with toxicant, while retaining much of their structure and function. Because CGCs at different stages of development appear to have differential sensitivities to MeHg, we sought to determine if there is a difference in response of $[Ca^{2+}]_i$ to acutely applied MeHg. We used the fluorescent indicator fluo4, which labels free divalent cations, to indicate relative changes in $[Ca^{2+}]_i$. In addition, we tested for the contribution of $GABA_A$Rs using the non-specific $GABA_A$R agonist and antagonist muscimol and bicuculline, respectively.

MATERIALS AND METHODS

Chemicals and solutions

Methylmercuric (II) chloride was obtained from Aldrich Chemical (Milwaukee, WI). Fluo4 (NW, no wash), ethidium homodimer-1 (ethD-1) and probenecid were obtained from Invitrogen Molecular Probes (Eugene, OR). Muscimol hydrobromide and bicuculline methobromide were obtained from Sigma Chemical Co. (St. Louis, MO).

Tissue dissections were carried out in a solution containing (in mM): 222.5, sucrose; 2.5, KCl; 4, $MgCl_2$; 1.25, KH_2PO_4; 26, $NaHCO_3$; 1, $CaCl_2$; and 25, D-glucose (pH 7.3-7.5 when oxygenated) at room temperature of 23-25 °C. These low [Na^+], low [Ca^{2+}], high [Mg^{2+}] slicing solutions were used to reduce cellular damage during slicing. Slices were kept in this solution for no longer than 15 min. Further incubations were performed in ACSF containing (in mM): 125, NaCl; 2.5, KCl; 1, $MgCl_2$; 1.25, KH_2PO_4; 26, $NaHCO_3$; 2, $CaCl_2$; and 20, D-glucose (pH 7.3-7.5 when oxygenated). ACSF was supplemented with MeHg from a 10 mM stock solution in double-distilled water for treatments. All working solutions were prepared within 48 h of use and oxygenated with 95/5% O_2/CO_2 at room temperature during treatments. 2X stock of fluo4 was prepared according to the supplier's instructions and diluted to a final concentration of 4 μM in ACSF supplemented with 2.5 μM probenecid to facilitate fluorophore loading (Mehlin *et al*., 2003). Stock solutions of 100 mM muscimol and 10 mM bicuculline were prepared in double-distilled water and stored at -20°C until use. Choice of concentrations of bicuculline and muscimol was based on previous electrophysiological experiments involving bath application of 100 μM or 10 μM bicuculline in hippocampal or cerebellar slices (Yuan and Atchison 1997, 2003), and optimizations showing a temporary increase in $[Ca^{2+}]_i$ from bath application of 100 μM muscimol in slices (Results not shown).

JPET Fast Forward. Published on October 29, 2015 as DOI: 10.1124/jpet.115.226761
This article has not been copyedited and formatted. The final version may differ from this version.

Acute slice preparation

All animal procedures are in accordance with NIH guidelines for experimental animal use and were approved by the Michigan State University Institutional Animal Care and Use Committee. Timed-pregnant, female Sprague-Dawley rats were obtained from Charles River Laboratories (Cambridge, MA). Pregnant and nursing dams were fed high-fat diets (Purina 7024, Land O Lakes Purina, Richmond, IN) to improve litter size. All rats were given doubly-distilled water to drink *ad libitum*.

Male and female rat pups (M=24, F=14, postnatal days 8-12) were euthanized by rapid decapitation. Their brains were rapidly removed. Cerebella were maintained in ice-cold, oxygenated solution during slicing. Sagittal slices 250 μm thick were cut using a Leica VT100S vibratome (Leica Microsystems Inc., Bannockburn, IL). After slicing, slices were incubated in oxygenated ACSF at room temperature for 1 h.

Incubations in ACSF alone were followed by incubations in fluorophores in ACSF, either for cytotoxicity assays or for time course studies. A live/dead assay consisting of fluo4/ethD-1 was used to determine if the concentrations of MeHg used in time course studies were lethal to cells in slices during the imaging period. Slices were incubated in ACSF with 1X fluo4 and 4 μM ethD-1 for 2 h (post-incubation control), for 3 h (+1 h ACSF) or for 3 h supplemented with 20 μM MeHg during the final h (+1 h MeHg). Due to time-constraints in imaging, these were not matched to the 40 min MeHg treatments of the time courses, but were kept to 60 min treatment and the highest concentration used in time course assays, 20 μM MeHg, to represent the maximal treatment tested. All other treatments incubated slices in ACSF with 1X fluo4 from 2-8 h as needed. In some cases, multiple slices from the same animal were used on a treatment day, but no slices from individual animals or animals in the same litter were given the same treatment.

Confocal Microscopy

For each treatment, a cerebellar slice was removed from fluorophore incubation and anchored in a microscope perfusion chamber with gravity-fed oxygenated ACSF flowing at 2-3 ml/min at room temperature, 23-25°C. Slices were visualized under 10X and 40X water immersion objectives (NA 0.3 and 0.8, respectively) fitted to an upright Leica TSL confocal scanning microscope (Leica Microsystems Inc., Bannockburn, IL). Magnified regions of the slices were examined using an argon laser at 488 nm excitation. To reduce the incidence of photobleaching, laser power was set at less than 30% of maximum. To maximize the number of cells available for analysis, 40X magnified regions were chosen that contained fluorescent cells in all cerebellar layers, based on initial visualization at 10X magnification.

Slices incubated for the cytotoxicity assays were sequentially scanned for fluo4 and ethD-1. Imaging was performed at 488 and 543 nm laser excitation with emission filters for fluo4 (500-535 nm) and ethD-1 (556-700 nm). For single-label experiments, a wider fluo4 emission could be sampled, so an emission filter of 500-700 nm was used. Imaging parameters for both fluorophores were scaled manually to the maximum and minimum saturation limits for pixel values before taking scans. Images were taken at a 512x512 pixel resolution representing a (300 μm)^2 field of view. The full thickness of each post-incubation slice, typically 100-160 μm, was scanned as a Z-series of images representing an image stack. Between-image depth was set at 3-5 μm to decrease imaging time and minimize photobleaching while still taking multiple images of each cell. Imaging of cytotoxicity assays included two regions of each slice, taken at 10X and 40X magnification. For time course experiments, one region of the slice was selected. To maintain visualization of the same cells through the experiment, framing of the image was manually reset between time points.

JPET Fast Forward. Published on October 29, 2015 as DOI: 10.1124/jpet.115.226761
This article has not been copyedited and formatted. The final version may differ from this version.

Several concentrations of MeHg were tested for effects on $[Ca^{2+}]_i$. In these time course treatments, two pretreatment time points (-10 and -5 min) established a baseline fluo4 signal, followed by 40 min of continuous perfusion with a single concentration of either 1, 5, 10 or 20 μM MeHg starting at 0 min. These concentrations are higher than those used for isolated cells in culture (Herden *et al.*, 2008) due to greater extent of non-specific binding of MeHg in tissue. They fall between 1 μM MeHg concentrations shown to allow cell survival and migration in rat cerebellar slice culture for several days (Mancini *et al*., 2010) and blood concentrations calculated in acute human exposures in Iraq, up to 19.5 μM (Bakir *et al*., 1973). Untreated control slices were used to monitor photobleaching with no MeHg treatment over the same time period. For all treatments, image stacks were collected every 5 min.

$GABA_AR$ function and divalent cation regulation was compared in the presence and absence of MeHg using muscimol and bicuculline, a nonspecific $GABA_AR$ agonist and antagonist, respectively. As in treatments with MeHg alone, images were collected at two pretreatment points, -10 and -5 min, and images were collected every 5 min thereafter for 40 min. For combination treatments, continuous perfusion with 20 μM MeHg started at t=0 min and slices were treated with four 60 sec pulses of either 100 μM muscimol or 10 μM bicuculline in ACSF. These treatments repeated addition of the same agent 30 sec before the 10, 20, 30 and 40 min time points to allow the perfusate to reach the slice in time for imaging. Bicuculline and muscimol controls were performed in which these agents were pulsed in the absence of MeHg. The 20 μM concentration of MeHg was used in combination treatments to allow for treatment comparison to an increase in $[Ca^{2+}]_i$ in all layers.

Image Analysis and Statistics

Cytotoxicity assay images were processed using Leica Confocal Software Lite (ver. 2.61, Leica Microsystems Heidelberg, GmbH). Histological layers were visualized and categorized

into EGL, ML or IGL based on fluo4 staining of CGCs (Fig. 1A). CGCs were identified as spherical cells up to 10 μm in diameter. The EGL, 10 to 30 μm thick, extended from the pial edges of the slice to the origin of dendritic processes (Figs. 1, 2). The ML, 60 to 80 μm thick, contained diffuse fluo4-stained PC dendrites and linear glial processes. CGCs located along the EGL/ML margin were considered EGL cells. A single layer of PCs divides the ML and IGL, but since PCs in this treatment do not typically appear to fluoresce with fluo4 treatment, the ML/IGL boundary was defined as the end of dendrite staining and the start of densely-packed fluorescent cells. Cells falling on the ML/IGL boundary were excluded from analysis because Purkinje cell processes and other fluorescent processes frequently overlapped with CGCs there. The IGL extended 60 to 80 μm from this line before an observable drop in fluo4 staining occurred, consistent with the edge of cerebellar white matter.

For cytotoxicity assays, regions of interest were delineated around each visible layer in 40X magnification image stacks, divided by visible boundaries denoted above (Fig 1). Histograms were taken for each layer region of interest, with the threshold for positive staining set at 10% of maximum pixel intensity. From each histogram, the sum of all pixels positive for ethD-1 was divided by the layer's total pixel area to produce ethD-1 pixel intensities, expressed as a percent. Each layer's pixel intensities from two 40X image stacks per slice were averaged to produce mean pixel intensities per animal, and then averaged per treatment. With only one confocal platform to image slices, the +1 h MeHg-treated slices and the +1 h ACSF-treated slices had to come from different animals, so an *n* of 1 represents all treatments from the same litter.

For time courses, image stacks were processed using ImageJ (Rasband, 2011, imagej.nih.gov/ij/). Background was subtracted from each image using the "Subtract

JPET Fast Forward. Published on October 29, 2015 as DOI: 10.1124/jpet.115.226761
This article has not been copyedited and formatted. The final version may differ from this version.

Background Tool" with a 50 pixel rolling-ball radius. Resulting images were divided into time points and projected to two dimensional images by summing the pixels in the z-dimension. These summed image series were aligned over time using the "StackReg" plugin (Thévenaz *et al*., 1998) and cropped to eliminate unused space, typically removing 10-12 pixels in each dimension. CGCs were chosen from all three layers, using the "elliptical brush tool" to select approximately 10 μm circles around distinguishable CGCs. Mean pixel intensities (F_t) from these CGCs as circular regions of interest were collected using the "Multi Measure" plugin (Rasband *et al*., 2006). Cells were classified into two categories. Cells that visibly lysed, visibly detached from the tissue, or lost fluo4 fluorescence between time points and did not recover were tallied as extinguished, as they either lost cell membrane integrity or detached from the tissue between time points. Significant fluorescence loss typical for extinguishing events was determined by finding negative change in fluorescence between time points (ΔF) significantly greater than the mean change of the cells in the same layer ($P<0.05$). Typical extinguishing events displayed >10% fluorescence loss, and were checked visually in the original images before discarding. All non-extinguishing mean pixel intensities were tracked for the time course. Pixel intensities were normalized to the average of two pretreatment intensities (F/F_0). Cell density (cells/(100 μm)^2) was determined from total cell counts, live and extinguished, corrected for layer areas using additional polygonal regions of interest in ImageJ. Tallies for extinguished cells were compared to total cells counted in each layer.

For cytotoxicity assays, cell densities and extinguished cell counts, paired mean comparisons were made in GraphPad Prism (v4.03, GraphPad Software, Inc., La Jolla, CA). For Ca^{2+} time course experiments, overall effects and interactions were determined using IBM SPSS Statistics (SPSS) (IBM, Somers, NY). Assays were analyzed using repeated measures ANOVA with layers and time as within-subjects factors (Steel and Torrie, 1960). Because of different numbers

of replicates in different groups (n=3 to 6), adjusted means were used for statistical comparisons. No treatment group included sufficient separate replicates of males and females to compare the two groups. Additionally, each treatment group was assessed separately for significant changes in F/F_0 over time and between layers. *Post-hoc* comparisons were made in SPSS for time and layer comparisons and GraphPad Prism for treatment comparisons. Bonferroni corrections were used for multiple treatment comparisons. All effects, interactions and comparisons were considered significant for $P<0.05$.

JPET Fast Forward. Published on October 29, 2015 as DOI: 10.1124/jpet.115.226761
This article has not been copyedited and formatted. The final version may differ from this version.

RESULTS

Visualization of layers and cytotoxicity

Fluo4 labeled mainly small (5-10 μm diameter), round somata matching the size and shape of CGCs (Fig. 1, 2). Larger cells were not typically labeled visibly with fluo4, similar to what was seen previously (Yuan and Atchison, 2007). Some processes were visible and were used to delineate boundaries of the ML (Fig. 1A). These processes include linear structures consistent with Bergmann glia and branching structures consistent with PC dendrites. Occasionally, cells visible at the boundary between the IGL and ML reacted fluorescently during treatment, usually around the addition of MeHg. These cells may be Bergmann glia or other interneurons present in this region that can be loaded with application of fluo4 (Hoogland *et al*., 2011). They were sufficiently different in shape and size so as not to be confused with CGCs. Fluo4-labeled CGCs were located in all three layers of the cerebellum. In the EGL, CGCs were concentrated at the pial surface and inner folds of lobes, but additional CGCs were located at the boundary between the EGL and ML. Most fluo4-labeled CGCs were situated in the IGL, evenly distributed throughout the slice thickness (Fig. 1). Comparatively few fluo4-labeled CGCs were located in the ML.

EthD-1 did not stain any fluo4-labeled cells, indicating that only viable cells accumulated the Ca^{2+} indicator fluo4 (Fig. 1A). In the absence of MeHg, EthD-1 intensity was 15.8% in the IGL, 13.8% in the ML and 16.1% in the EGL at the post-incubation time point matching the start of time course imaging, so ethidium staining was similar in all three layers (Fig. 1B). This presumably reflects cell damage due to slicing and the incubation process. Slices imaged after one additional h of untreated incubation, corresponding to the end of a time course treatment, were not different in ethD-1 mean pixel intensity, indicating there is not a significant change in slice viability within the time frame used. In slices incubated for 3 h in fluorophore plus 20 μM

MeHg for 1 h, roughly corresponding to slices incubated in MeHg for a time course series, there was an increase in ethD-1 staining in the EGL when compared to untreated slices after 3 h of incubation, but it was not different from ethD-1 staining with one additional h of fluorophore incubation. Thus MeHg appears to exacerbate cell death induced by slicing in the EGL, but does not increase the incidence of cell death over slicing alone for the short incubation times used in these experiments.

Acute MeHg slice treatment

Relative pixel fluo4 fluorescence intensity (F/F_0), a measure of changes to $[Ca^{2+}]_i$, was unaltered over 40 min in slices in the absence MeHg treatment. Changes in mean F/F_0 in cells did not exceed 5% between any two consecutive time points. Thus, none of the observed effects were due to photobleaching of fluo4 during confocal imaging (Figs. 2, 3).

Effects of MeHg on $[Ca^{2+}]_i$ in CGCs were dependent upon concentration and differed by histological layer. In all treatments with MeHg, the greatest effect on fluorescence occurred in the EGL, and decreased in magnitude in the deeper layers (Fig. 4). In slices treated with MeHg, all regions appeared to increase in fluorescence over the treatment period, including the processes distributed through the ML (Fig. 2).

After a 40 min exposure to 20 μM MeHg, fluo4 F/F_0 was significantly increased in CGCs in all three layers, with a significantly larger effect in the EGL compared to deeper laminae (Figs. 2, 3). This MeHg concentration increased mean F/F_0 up to 263% of baseline in the EGL, 186% in the ML and 173% in the IGL. At 10 μM MeHg, CGC F/F_0 increased to 192% baseline in the EGL, 142% in the ML and 164% in the IGL. In the EGL and ML, 20 μM MeHg increased F/F_0 significantly more than 10 μM MeHg. Perfusion with 1 or 5 μM MeHg produced no increases in F/F_0 compared to untreated control in any layer over this interval of recording. The

JPET Fast Forward. Published on October 29, 2015 as DOI: 10.1124/jpet.115.226761
This article has not been copyedited and formatted. The final version may differ from this version.

largest changes in fluorescence occurred before the 20 min time point. They included a 43% increase in fluorescence relative to F_0 in the EGL between 10 and 15 min time points when treated with 20 μM MeHg.

Calculating fluorescent changes relies heavily on the number of cells being tracked, and it appeared that MeHg treatment increased the number of cells that were visible during treatment. This was reflected in the density of cells that could be counted in layers. In untreated slices, 37 ± 2 CGCs per $(100\ \mu m)^2$ were visualized in the IGL over the full course of treatment, 5 ± 1 in the ML and 16 ± 2 in the EGL (Fig. 4). Regardless of treatment, cells in the IGL were more densely distributed than in the other two histological layers. There was an increase in the density of CGCs visible in slices treated with 10 or 20 μM MeHg, most notably in the EGL, where visible CGCs increased to a density of 63 ± 7 per $(100\ \mu m)^2$ (Fig. 4). Many of the cells tracked in these MeHg treatments were not initially visible at pretreatment time points, but could be tracked due to the registration of images. While increased cell count in MeHg treatments meant comparative difficulty tracking of CGCs in low and no-MeHg treatments with low baseline fluorescence, with the careful setup of the slices there were always enough visible CGCs for tracking in all slices and layers.

Some CGCs appeared to extinguish fluorescence during 50 min of imaging. Considerable effort was made to track and exclude these CGCs from the remaining population trend lines, as a drop in fluorescence in enough cells could diminish the measured effect of increasing fluorescence. These CGCs lost fluorescence suddenly as compared to other cells in their layer and such outliers were thus excluded from fluorescence intensity measurements. These outliers made up 17.7% of total CGCs (Fig. 5), indicating a substantial number of extinguishing cells. These extinguished cells were occasionally accompanied by visible lysis or detachment from surrounding tissue, but evidence of these mechanisms is lost between imaging time points for

most of the extinguished cells. This number matches well with the percentages of dead cells from the previous cytotoxicity assay, so this percent of cell loss indicates a baseline rate of cell loss during experiments due to imaging and perfusion of buffer over the slices.

Muscimol and bicuculline treatment with MeHg

Both the muscimol (100 μM) and bicuculline (10 μM) delayed the onset and partially reduced the magnitude of effect of MeHg on fluo4 fluorescence in CGCs over time (Figs. 6, 9). However neither agent prevented the increases caused by MeHg. Moreover, the effects of $GABA_AR$ modulation were developmental layer-dependent. For example, in the presence of muscimol, MeHg treatment increased F/F_0 up to 208% of baseline in the EGL, 148% of baseline in the ML and 141% of baseline in the IGL. The magnitudes of these increases were significantly ($p< 0.05$) less than those produced by MeHg alone in each layer by the end of treatment (Fig. 6). Similarly bicuculline pulses combined with MeHg resulted in increases of F/F_0 to 211% of baseline in the EGL, 149% of baseline in the ML, and 157% of baseline in the IGL; for the EGL and ML, these increases in fluorescence were significantly less than those caused by MeHg alone (Fig. 6). In the IGL, where MeHg alone was less effective in stimulating fluo4 fluorescence, bicuculline did not significantly reduce the increase in F/F_0 caused by MeHg, but did delay its onset from 15 to 35 min of MeHg treatment, similar to its effect in other layers. Neither muscimol nor bicuculline alone altered fluo4 fluorescence over the duration of treatments ($p > 0.05$).

When examining the effects of $GABA_AR$ modulation on fluorescence cell density, a somewhat different pattern was seen. Again, neither agent alone altered the number of cells which experienced spontaneous fluorescence, but whereas the agonist reduced the fluorescence

JPET Fast Forward. Published on October 29, 2015 as DOI: 10.1124/jpet.115.226761
This article has not been copyedited and formatted. The final version may differ from this version.

cell density in response to MeHg, bicuculline was ineffective (Figs. 7, 10). Bicuculline did not change extinguished cell counts from controls (Fig. 8). Furthermore the effects of muscimol on levels of extinguished cell counts was again layer-dependent, however in this case muscimol was only effective in quenching the effects of MeHg in the ML and IGL (Fig. 11).

DISCUSSION

The present study was designed to begin to examine the relationship between the developmental stage of CGCs and susceptibility to MeHg-induced dysregulation of intracellular divalent cation regulation. Moreover, because $GABA_A$Rs exhibit both high sensitivity to MeHg (Yuan *et al.*, 2005; Herden *et al.*, 2008), and developmental stage-dependence (Takayama and Inoue, 2004a), we examined the prospective role which these crucial receptors might play in the response to MeHg. The results show that 1) MeHg application triggers rapid and sustained increases in CGC $[Ca^{2+}]_i$ during development, 2) these changes are variable based on the developmental stage of the CGCs in slices, and 3) the disruption of $[Ca^{2+}]_i$ is regulated in part by activity of $GABA_A$Rs. The concentrations of MeHg used did not decrease cell viability during the time of exposure compared to slicing alone, as indicated by the cytotoxicity assay, though the large increases in $[Ca^{2+}]_i$ could affect viability at later time points. These MeHg concentrations are consistent with those which increase release of both excitatory and inhibitory transmitters in mature rodent cerebellar slices (Yuan and Atchison, 2003, 2007). Slice culture allowed for conditions similar to cell culture and a basic concentration/response assessment for this tissue and treatment. Both 10 and 20 μM MeHg caused intense increases in fluorescence while 5 and 1 μM did not in the time course studied. Importantly, we showed differences in response between CGCs at different developmental stages of migration. The basic disruption of $[Ca^{2+}]_i$ shown here is consistent with previous measurements showing these increases are an initial mechanism of MeHg toxicity in CGCs (Marty and Atchison, 1998, Limke *et al*., 2003, Edwards *et al*., 2005). We further showed that modulators of $GABA_A$Rs are capable of altering increases in $[Ca^{2+}]_i$ rapidly as well, effectively decreasing and delaying the MeHg-induced increases.

Increases in $[Ca^{2+}]_i$ are a consistent effect of MeHg, being seen in single neurons in

JPET Fast Forward. Published on October 29, 2015 as DOI: 10.1124/jpet.115.226761
This article has not been copyedited and formatted. The final version may differ from this version.

culture (Hare *et al.*, 1993; Marty and Atchison, 1997; Bemis and Seegal, 2000; Limke and Atchison, 2001; Edwards *et al.*, 2005), acutely exposed cerebellar slices (Yuan and Atchison, 2007), synaptosomes (Denny *et al.*, 1993; Dreiem and Seegal, 2007), and even in mice treated chronically with MeHg (Johnson *et al.*, 2011). Moreover, this effect occurs early in exposure, requiring neither extended exposure, nor high MeHg concentrations, as pharmacokinetic barriers to MeHg absorption and distribution are negated *in vitro*. In these *in vitro* systems, the kinetic profile of this Ca^{2+} response has been studied in considerable detail (Hare *et al.*, 1993; Hare and Atchison, 1995a,b; Marty and Atchison, 1997; Limke and Atchison, 2001; Limke *et al.*, 2003, 2004; Edwards *et al.*, 2005). It comprises a multiphasic response with temporally distinct phases which reflect initially release of Ca^{2+}_i from internal stores in mitochondria and endoplasmic reticulum (Hare *et al.*, 1993; Hare and Atchison, 1995a,; Marty and Atchison, 1997; Limke and Atchison, 2001; Limke *et al.*, 2003, 2004), and subsequent entry of Ca^{2+} through pathways controlled by VGCCs (Hare and Atchison, 1995b; Marty and Atchison, 1997), glutamate receptors (Ramanathan and Atchison, 2011, Johnson *et al.*, 2011), and cholinergic nicotinic (unpublished observations) and muscarinic (Limke *et al.*, 2004) receptors. We now extend that observation, most importantly to $GABA_A$ receptors.

Effects of MeHg on CGCs during migration can clearly be attenuated by $GABA_AR$ modulation, indicating that the receptor can be affected in any stage of development, and supporting a role for $GABA_ARs$ in immediate mechanisms of MeHg toxicity. $GABA_AR$ modulation by either agent does not abolish the effects of MeHg, indicating there are likely other mechanisms occurring simultaneously. This is not surprising as other effects, such as those on VGCCs and muscarinic receptors, are also likely to occur rapidly (Sirois and Atchison, 2000; Limke *et al.*, 2004; Roda *et al.*, 2008). Moreover, muscimol appears to be acting similarly to bicuculline over the longer time courses, in that both reduce the effect of MeHg on $[Ca^{2+}]_i$.

JPET Fast Forward. Published on October 29, 2015 as DOI: 10.1124/jpet.115.226761
This article has not been copyedited and formatted. The final version may differ from this version.

Multiple mechanisms could be responsible for a similar action of muscimol and bicuculline. If both are acting as competitive antagonists to MeHg, then both would appear to decrease the effect of MeHg, but the two agents act at slightly different sites and the muscimol site activates even if MeHg is bound (Fonfría *et al*., 2001). Those binding studies assumed an incubation with the agents first. In this study MeHg is applied first, so competition might be different. The reduction in effect by both an agonist and an antagonist could also be due to the nature of most agonists, in that the initial pulse increases conductance transiently, but is followed by lingering desensitization, so we only observe the effects of overall antagonism. Whatever the mechanism, there are a few subtle differences in this study between bicuculline and muscimol. First, the combination of bicuculline and MeHg was indistinguishable from MeHg alone in causing changes in visible density of fluorescent cells, whereas the combination with muscimol decreased this density in the EGL but increased it in the IGL. Second, the combination of MeHg and muscimol pulses increased cytotoxicity as measured by extinguished cells in this study where bicuculline did not. If muscimol transiently increases $[Ca^{2+}]_i$ that is not detectable by these imaging parameters, it is possible that it contributes to MeHg cytotoxicity despite lowering the observed overall $[Ca^{2+}]_i$ in most cells.

The differences in effectiveness of muscimol and bicuculline as a function of developmental layer were not sufficiently large as compared to MeHg to suggest that one type of agent is more effective in one layer than another. As the surface expression of receptor subunits such as α6, α2, γ and δ changes over development (Beattie and Siegel, 1993; Zheng *et al.*, 2003), the agents either function similarly regardless of the expression profiles of the CGCs, or specific reactions are lost in the variability of the populations. It would be possible to treat slices with more specific $GABA_AR$ modulators, such as those targeting the α6 or δ subunit, but the

JPET Fast Forward. Published on October 29, 2015 as DOI: 10.1124/jpet.115.226761
This article has not been copyedited and formatted. The final version may differ from this version.

variability of the receptors (Nusser *et al.*, 1998) and the population of CGCs would complicate interpretation of these results.

A tightly regulated amount of free $[Ca^{2+}]_i$, is critical to driving migration and maturation of CGCs (Komuro and Rakic, 1992, Kumada and Komuro, 2004). As with all neurons, a sustained increase or inability to buffer $[Ca^{2+}]_i$ can lead to activation of cell death pathways, including caspases, cytoskeletal breakdown and opening of the mitochondrial transition pore (Fonfría *et al*., 2002, Limke and Atchison, 2002, Limke *et al*., 2003, Roda *et al*., 2008). Critical cycling of increased $[Ca^{2+}]_i$ in CGC migration is another potential susceptibility to MeHg. Continuous increases in $[Ca^{2+}]_i$ from the addition of caffeine or thimerosal, another mercury-based compound, disrupt migration of CGCs (Kumada and Komuro 2004, Komuro and Kumada 2005). Normal physiological changes in $[Ca^{2+}]_i$, as would be seen using electrophysiological current recordings are small, transient, and occur too rapidly to be captured by this confocal microscopy setup. Even a temporary increase in $[Ca^{2+}]_i$ could have profound effects on cell survival.

In these MeHg treatments, the $[Ca^{2+}]_i$ levels in CGCs increased dramatically, but $[Ca^{2+}]_i$ in PCs and other cells present in the slices did not label to any significant degree. This difference in cell body labeling reflects cell susceptibility and underscores the importance of $[Ca^{2+}]_i$ in studying MeHg toxicity. Since the largest $[Ca^{2+}]_i$ changes in CGCs for many treatments were at the end of recording, the concentration may continue to rise and may eventually fall before cell death, as has been seen in previous studies (Yuan and Atchison, 2007). This may occur even for those levels of MeHg which did not reach significance in these experiments. Extending the treatment and monitoring might allow such increases to be seen, but could be complicated by the slow export of fluo4 or the continued extinguishing of fluorescence by dead or dying cells.

Clinical manifestations of MeHg poisoning and the susceptibility of human fetuses point

JPET Fast Forward. Published on October 29, 2015 as DOI: 10.1124/jpet.115.226761
This article has not been copyedited and formatted. The final version may differ from this version.

strongly to the migration of CGCs in the cerebellum as being a particularly sensitive target for MeHg toxicity. We categorized CGCs into those that were still dividing, those that were migrating and those that had reached their destination based on their location within the cerebellum. In MeHg treatments, fluorescence changes were distinct in the different layers; the more mature CGCs in the ML and IGL reacted less to MeHg than did migrating CGCs as indicated by changes in their F/F_0. Regardless of the mechanisms, this indicates that immature CGCs experience a larger sustained increase in $[Ca^{2+}]_i$ as an early exposure event than more mature cells.

Even if early free Ca^{2+} is sequestered, lasting disruption of cell signaling is possible. Precise signaling is particularly important for the migration of CGCs; fewer CGCs reaching their target layer and maturing means fewer circuits made. The CGC and PC circuit is the major internal cerebellar neuronal circuit; since many CGCs normally synapse on PCs, their signal can be integrated over a population of the cells. If the population of CGCs is reduced, there is both a larger load placed on any individual CGC as well as poorer integration of signal. This can have lasting consequences long after the initial exposure, including motor coordination and motor memory deficits related to the overall function of the cerebellum. Since MeHg is persistent in brain tissue, if it is present in the brain during development it may continue to be toxic beyond the most susceptible developmental period.

While some exploration of the mechanisms of acute MeHg toxicity focuses on various VGCCs or reactive oxygen species production, the results presented here indicate additional acute effects via $GABA_A$Rs on $[Ca^{2+}]_i$. An identical pattern of action of bicuculline and muscimol on migration and Ca^{2+} regulation has been described for the neocortex (Heck et al., 2007). Thus the effects seen with the agonist and antagonist in combination with MeHg are not

JPET Fast Forward. Published on October 29, 2015 as DOI: 10.1124/jpet.115.226761
This article has not been copyedited and formatted. The final version may differ from this version.

unique. GABA is the major inhibitory neurotransmitter in the central nervous system, and has several roles in cerebellar circuitry, so evidence of the involvement of $GABA_A$Rs in the toxicity of MeHg must be taken into account in the study of the toxicant. The results presented here support initial electrophysiological findings (Yuan and Atchison, 2003, 2007), binding studies (Corda, *et al*., 1981, Fonfría, *et al*., 2001), and other toxicological studies (Basu, *et al*., 2010) in indicating a role here for $GABA_A$Rs and might explain known cellular and developmental susceptibilities to MeHg. Though this work focuses on only acute effects over less than 1 h of MeHg treatment, $GABA_A$Rs respond to stressors with changes in surface expression (Mhatre et al., 1993; Saliba et al., 2009), indicating that acute effects could trigger longer-term effects as well. Whether the effects of MeHg on $GABA_A$Rs are acute or chronic, the sensitive migration and maturation of CGCs is affected, potentially contributing to the susceptibility of these cells at a crucial point in development.

ACKNOWLEDGMENTS

We would like to thank Drs. Stephen Schneider, Cheryl Sisk and Ravindra Hajela for help with writing and editing the manuscript and Dr. Dirk Colbry for training in image processing and analysis. Jessica Gevers assistance with illustrations and word processing is appreciated as well.

JPET Fast Forward. Published on October 29, 2015 as DOI: 10.1124/jpet.115.226761
This article has not been copyedited and formatted. The final version may differ from this version.

AUTHORSHIP CONTRIBUTIONS

Participated in research design: Bradford, Mancini and Atchison.

Conducted experiments: Bradford and Mancini.

Contributed new reagents or analytic tools: Bradford

Performed data analysis: Bradford, Mancini and Atchison.

Wrote or contributed to the writing of the manuscript: Bradford, Mancini and Atchison.

REFERENCES

Amin-Zaki, L, Elhassani, S, Majeed, MA, Clarkson, TW, Doherty, RA, and Greenwood, M (1974) Intra-uterine methylmercury poisoning in Iraq. *Pediatrics* **54,** 587-595.

Bakir, F., Damluji, S.F., Amin-Zaki, L., Murtadha, M., Khalidi, A., Al-Rawi, N.Y., Tikriti, S., Dhahir, HI, Clarkson, TW, Smith, JC, and Doherty, RA (1973) Methylmercury poisoning in Iraq. *Science* **181,** 230-241.

Basu N, Scheuhammer AM, Rouvinen-Watt K, Evans RD, Trudeau VL and Chan LH (2010) In vitro and whole animal evidence that methylmercury disrupts GABAergic systems in discrete brain regions in captive mink. *Compar Biochem Physiol Toxicol Pharmacol* **151**:379-385.

Beattie CE, Siegel RE (1993) Developmental cues modulate $GABA_A$ receptor subunit mRNA expression in cultured cerebellar granule neurons *J Neurosci.* **13,** 1784-1792.

Bemis JC and Seegal RF (2000) Polychlorinated biphenyls and methylmercury alter intracellular calcium concentrations in rat cerebellar granule cells. *NeuroToxicology* **21,**1123-1134.

Corda MG, Concas A, Rossetti Z, Guarneri P, Corongiu FP and Biggio G (1981) Methyl mercury enhances [^{3}H]diazepam binding in different areas of the rat brain. *Brain Res* **229,**264-269.

Denny MF, Hare MF and Atchison WD (1993) Methylmercury alters intrasynaptosomal concentrations of endogenous polyvalent cations. *Toxicol Appl Pharmacol* **122,** 222-232.

Dreiem A and Seegal RF (2007) Methylmercury-induced changes in mitochondrial function in striatal synaptosomes are calcium-dependent and ROS-independent. *NeuroToxicology* **28**:720-726.

Edwards, JR, Marty, MS, and Atchison, WD (2005) Comparative sensitivity of rat cerebellar neurons to dysregulation of divalent cation homeostasis and cytotoxicity caused by methylmercury. *Toxicol Appl Pharmacol* **208,** 222-232.

Fonfría, E, Rodriguez-Farre, E, and Suñol, C (2001) Mercury interaction with the $GABA_A$ receptor modulates the benzodiazepine binding site in primary cultures of mouse cerebellar granule cells. *Neuropharmacology* **41,** 819-833.

Fonfría, E, Dare, E, Benelli, M Suñol, C, and Ceccatelli, S (2002) Translocation of apoptosis-inducing factor in cerebellar granule cells exposed to neurotoxic agents inducing oxidative stress. *Eur J Neurosci* **16,** 2013-2016.

Hajela, RK, Peng, SQ, and Atchison, WD (2003) Comparative effects of methylmercury and Hg^{2+} on human neuronal N- and R- type high-voltage activated calcium channels transiently expressed in Human Embryonic Kidney 293 cells. *J Pharmacol Exp Ther* **306,** 1129-1136.

Hare MF and Atchison WD (1995a) Methylmercury mobilizes Ca^{++} from intracellular stores sensitive to inositol 1,4,5-trisphosphate in NG108-15 cells. *J Pharmacol Expt Ther* **272,** 1016-1023.

Hare MF, Atchison WD (1995b) Nifedipine and tetrodotoxin delay the onset of methylmercury-induced increase in $[Ca^{2+}]_i$ in NG108-15 cells *Toxicol Appl Pharmacol* **135,** 299-307.

Hare MF, McGinnis KM and Atchison WD (1993) Methylmercury increases intracellular concentrations of Ca^{++} and heavy metals in NG108-15 cells. *J Pharmacol Exp Ther* **266,**1626-1635.

Heck N, Kilb W, Reiprich P, Kubota H, Furukawa T, Fukuda A and Luhmann HJ (2007) GABA-A receptors regulate neocortical neuronal migration in vitro and in vivo. *Cerebr Cort* **17,** 138-148.

Herden, CJ, Pardo, NE, Hajela, RK, Yuan, Y, and Atchison, WD (2008) Differential effects of methylmercury on γ-aminobutyric acid type A receptor currents in rat cerebellar granule and cerebral cortical neurons in culture. *J Pharmacol Exp Ther* **324,** 517-528.

Hoogland, TM, Kuhn, B, and Wang, SS (2011) Preferential loading of Bergmann glia with synthetic acetoxymethyl calcium dyes. *Cold Spring Harb Protoc* **2011,** 1228-1231.

Hunter, D, and Russell, DS (1954) Focal cerebral and cerebellar atrophy in a human subject due to organic mercury compounds. *J Neurol Neurosurg Psychiat* **17,** 235-241.

Inoue M, Harada K, Nakamura J and Matsuoka H (2013) Regulation of α3-containing $GABA_A$ receptors in guinea-pig adrenal medullary cells by adrenal steroids. *Neuroscience* **253,** 245-255.

Johnson FO, Yuan Y, Hajela RK, Chitrakar A, Parsell DM and Atchison WD (2011) Exposure to an environmental neurotoxicant hastens the onset of amyotrophic lateral sclerosis-like phenotype in human Cu^{2+}/Zn^{2+} superoxide dismutase 1 G93A mice: glutamate-mediated excitotoxicity. *J Pharmacol Exp Ther* **338,** 518-527.

Komuro, H, and Kumada, T (2005) Ca^{2+} transients control CNS neuronal migration. *Cell Calcium* **37,** 387-393.

Komuro H, and Rakic, P (1992) Selective role of N-type calcium channels in neuronal migration. *Science* **257,** 806–809.

Komuro H, and Rakic P (1993) Modulation of neuronal migration by NMDA receptors. *Science* **260,** 95-97.

Komuro H, Rakic P (1995) Dynamics of granule cell migration: A confocal microscopic study in acute cerebellar slice preparations. *J Neurosci* **15,** 1110–1120.

Komuro, H, and Rakic, P (1998) Distinct modes of neuronal migration in different domains of developing cerebellar cortex. *J Neurosci* **18,**1478-1490.

Komuro Y, Galas L, Lebon A, Raoult E, Fahrion JK, Tilot A, Kumada T, Ohno N, Vaudry D and Komuro H (2015) The role of calcium and cyclic nucleotide signaling in cerebellar granule cell migration under normal and pathological conditions. *Developm Neurobiol* **75,** 369-87.

Kumada, T, and Komuro, H (2004) Completion of neuronal migration regulated by loss of Ca(2+) transients. *Proc Natl Acad Sci USA* **101**:8479–8484.

Kunimoto M and Suzuki T (1997) Migration of granule neurons in cerebellar organotypic cultures is impaired by methylmercury. *Neurosci Lett* **226,**183-186.

Laurie DJ, Seeburg PH, Wisden W (1992) The distribution of 13 $GABA_A$ receptor subunit mRNAs in the rat brain. II. Olfactory bulb and cerebellum *J Neurosci.* **12,** 1063-1076.

Limke, TL, and Atchison, WD (2002) Acute exposure to methylmercury opens the mitochondrial permeability transition pore in rat cerebellar granule cells. *Toxicol Appl Pharmacol* **178,** 52-61.

Limke, TL, Bearss, JJ, and Atchison, WD (2004) Acute exposure to methylmercury causes Ca^{2+} dysregulation and neuronal cell death in rat cerebellar granule cells through an M_3 muscarinic receptor-linked pathway. *Toxicol Sci* **80,** 60-68.

Limke, TL, Otero-Montañez, JK, and Atchison, WD (2003) Evidence for interactions between intracellular calcium stores during methylmercury-induced intracellular calcium dysregulation in rat cerebellar granule cells. *J Pharmacol Exp Ther* **304,** 949-958.

Mancini JD and Atchison WD (2007) The NR2B subunit in NMDA receptors is functionally important during cerebellar granule cell migration. *Neurosci Lett* **429,** 87-90.

Mancini, JD, Autio, DM, and Atchison, WD (2010) Continuous exposure to low concentrations of methylmercury impairs cerebellar granule cell migration in organotypic slice culture. *NeuroToxicology* **30,** 203-208.

Marty MS and Atchison WD (1997) Pathways mediating Ca^{2+} entry in rat cerebellar granule cells following in vitro exposure to methyl mercury. *Toxicol Appl Pharmacol* **147**:319-330.

Marty, MS, and Atchison, WD (1998) Elevations of Ca^{2+} as a probable contributor to decreased viability in cerebellar granule cells following acute exposure to methylmercury. *Toxicol Appl Pharmacol* **150,** 98-105.

Mehlin, C, Crittenden, C, and Andreyka, J (2003) No-wash dyes for calcium flux measurement. *BioTechniques* **34,** 164-166.

Mhatre MC, Pena G, Sieghart W, and Ticku MK (1993) Antibodies specific for $GABA_A$ receptor a subunits reveal that chronic alcohol treatment down-regulates α-subunit expression in rat brain regions. *J Neurochem*. **61,**1620–1625.

Mikawa S, Wang C, Shu F, Wang T, Fukuda A, Sato K (2002) Developmental changes in KCC1, KCC2 and NKCC1 mRNAs in the rat cerebellum *Dev Brain Res.* **136,** 93-100.

Nusser, Z, Sieghart, W, and Somogyi, P (1998) Segregation of different $GABA_A$ receptors to synaptic and extrasynaptic membranes of cerebellar granule cells. *J Neurosci* **18,** 1693-1703.

Owens, DF, Boyce, LH, Davis, MBE, and Kriegstein, AR (1996) Excitatory GABA responses in embryonic and neonatal cortical slices demonstrated by gramicidin perforated-patch recordings and calcium imaging. *J Neurosci* **16,** 6414-6423.

Peng, SQ, Hajela, RK, and Atchison, WD (2002) Effects of methylmercury on human neuronal L-type calcium channels transiently expressed in Human Embryonic Kidney cells (HEK-293) *J Pharmacol Exp Ther* **302,** 424-432

Philbert MA, Billingsley ML and Reuhl KR (2000) Mechanisms of injury in the central nervous system. *Toxicolog Pathol* **28,** 43-53.

Ramanathan G and Atchison WD (2011) Ca^{2+} entry pathways in mouse spinal motor neurons in culture following in vitro exposure to methylmercury. *NeuroToxicology* **32**:742-750.

Rasband, WS "ImageJ", US National Institutes of Health, Bethesda, Maryland, USA,1997-2011. rsb.info.nih.gov/ij/index.html Accessed 17 April 2012.

Rasband, W, Dougherty, B, Collins, T, Karperian, A and Stervbo, U "Multi-Measure" Optinav, Inc. 2006. www.optinav.com/imagej.html accessed 17 April 2012.

Rice, D, and Barone, S Jr. (2000) Critical periods of vulnerability for the developing nervous system: evidence from human and animal models. *Environ Health Perspect* **108,** Suppl:511-533.

Roda, E, Coccini, T, Acerbi, D, Castoldi, A, Bernocchi, G, and Manzo, L (2008) Cerebellum cholinergic muscarinic receptor (subtype-2 and -3) and cytoarchitecture after developmental exposure to methylmercury: an immunohistochemical study in rat. *J Chem Neuroanat* **35,** 285-294.

Sakamoto, M, Wakabayashi, K, Kakita, A, Takahashi, H, Adachi, T, and Nakano, A (1998) Widespread neuronal degeneration in rats following oral administration of methylmercury during the postnatal development stage: a model of fetal-type Minamata disease. *Brain Res* **784,** 351-354.

Sakamoto, M, Kakita, A, de Oliviera, RB, Pan, HS, and Takahashi, H (2004) Dose-dependent effects of methylmercury administered during neonatal brain spurts in rats. *Dev Brain Res* **152,** 171-176.

Saliba RS1, Gu Z, Yan Z, Moss SJ. (2009) Blocking L-type voltage-gated Ca^{2+} channels with dihydropyridines reduces gamma-aminobutyric acid type A receptor expression and synaptic inhibition. *J Biol Chem* **284,** 32544-32550.

Shafer TJ and Atchison WD (1991) Methylmercury blocks N- and L-type Ca^{++} channels in nerve growth factor-differentiated pheochromocytoma (PC12) cells. *J Pharmacol Expt Ther* **258,** 149-157.

Sirois, JE, and Atchison, WD (2000) Methylmercury affects multiple subtypes of calcium channels in rat cerebellar granule cells. *Toxicol Appl Pharmacol* **167,** 1-11.

Steel, RGD, and Torrie, JH (1960) Principles and procedures of statistics. New York: McGraw.

Takayama, C, and Inoue, Y (2004a) Transient expression of $GABA_A$ receptor α2 and α3 subunits in differentiating cerebellar neurons. *Dev Brain Res* **148,**169-177.

Takayama C, and Inoue Y (2004b) Morphological development and maturation of the GABAergic synapses in the mouse cerebellar granular layer. *Dev Brain Res* **150,** 177-190.

Takayama, C, and Inoue, Y (2006) Developmental localization of potassium chloride co-transporter 2 in granule cells of the early postnatal mouse cerebellum with special reference to the synapse formation. *Neuroscience* **143,** 757-767

Takeuchi, T, Morikawa, N, Matsumoto, H, and Shiraishi, Y (1962) A pathological study of Minamata Disease in Japan. *Acta Neuropathologica* **2,** 40-57

Thévenaz, P, Ruttimann, UE, and Unser, M (1998) A pyramid approach to subpixel registration based on intensity. *IEEE Trans on Image Proc* **7,** 27-41

Yamada, J, Okabe, A, Toyoda, H, Kilb, W, Luhmann, HJ, and Fukuda, A (2004) Cl^- uptake promoting depolarizing GABA actions in immature rat neocortical neurones is mediated by NKCC1. *J Physiol (Lond)* **557,** 829-841

Yuan, Y, and Atchison, WD (1997) Action of methylmercury on $GABA_A$ receptor-mediated inhibitory synaptic transmission is primarily responsible for its early stimulatory effects on hippocampal CA1 excitatory synaptic transmission. *J Pharmacol Exp Ther* **282,** 64-73.

Yuan, Y, and Atchison, WD (2003) Methylmercury differentially affects $GABA_A$ receptor-mediated spontaneous IPSCs in Purkinje and granule cells of rat cerebellar slices. *J Physiol (Lond)* **550,** 191-204.

Yuan Y, Otero-Montañez JK, Yao A, Herden CJ, Sirois JE, and Atchison WD (2005) Inwardly rectifying and voltage-gated outward potassium channels exhibit low sensitivity to methylmercury. *Neurotoxicology* **26,** 439-454.

Yuan, Y, and Atchison, WD (2007) Methylmercury-induced increase of intracellular Ca^{2+} increases spontaneous synaptic current frequency in rat cerebellar slices. *Mol Pharmacol* **71,** 1109-1121.

Zheng, T., Santi, MR, Bovolin, P, Marlier, LNJ, and Grayson, DR (2003) Developmental expression of the α6 $GABA_A$ receptor subunit mRNA occurs only after cerebellar granule cell migration. *Dev Brain Res* **75,** 91-103.

JPET Fast Forward. Published on October 29, 2015 as DOI: 10.1124/jpet.115.226761
This article has not been copyedited and formatted. The final version may differ from this version.

FOOTNOTES

This work was supported by the National Institute of Environmental Health Sciences Research Grant [R01-ES003299-23], Institutional Training Grant [T32ES007255-27]; the Johns Hopkins University Center for Alternatives to Animal Testing; and funds from the Michigan State University College of Osteopathic Medicine to support the D.O./Ph.D. training of JDM.

This work was submitted by ABB in partial fulfillment of the requirements of the Ph.D. in Biochemistry and Molecular Biology and Environmental Toxicology at Michigan State University.

Current address for ABB is: US Army Medical Research Institute of Chemical Defense, Gunpowder, MD, 21010

Current address for JDM is: NYIT College of Osteopathic Medicine Department of Osteopathic Manipulative Medicine

FIGURE LEGENDS

Figure 1. A Representative pseudocolor fluorescent image of an acutely-isolated cerebellar slice from PND9 rat showing modified fluo4/ethD-1 live/dead cytotoxicity assay, post-incubation control. Images are from internal folds of the developing cerebellum. Images show maximum fluo4 and ethD-1 fluorescence values by pixel. Approximate pial surface of an inner fold is indicated by a white line and other boundaries are indicated by dashed lines. EthD-1 (red), an indicator of dead cells, and Fluo4AM (green), an indicator of relative intracellular calcium concentration, do not colocalize. Scale bar represents 30 μm. **B** Representative image from separate slice from the same cerebellum after one additional h in ACSF supplemented with 20 μM MeHg. **C.** EthD-1 mean pixel staining (% pixels ± SEM) comparison of layers post-incubation in fluo4 and ethD-1 (n=5), with an additional 1 h incubation in ACSF (n=3) or with an additional 1 h incubation in 20 μM MeHg ACSF (n=3) Abbreviations: EGL, external granule layer; ML, molecular layer; IGL, internal granule layer.

Figure 2. 40X grayscale examples of cerebellar slices before (-10) and after (40 min) treatment with MeHg. Images show projection of maximum fluo4 fluorescence by pixel. **A.** Fluorescence does not change over the course of imaging in control slices. **B.** MeHg increased fluorescence in all layers, with the signal from many cells saturating the detector. Scale bars are 60 μm in all images. Surfaces and boundaries are indicated as with Figure 1. White arrows indicate examples of cells with extinguished fluorescence by the end of treatment.

JPET Fast Forward. Published on October 29, 2015 as DOI: 10.1124/jpet.115.226761
This article has not been copyedited and formatted. The final version may differ from this version.

Figure 3. Relative fluo4 fluorescence intensity (F/F_0) in CGCs by histological layer in slices from neonatal rat cerebellum exposed to concentrations of MeHg continuously for 30 min. Control MeHg concentrations did not change fluorescence significantly. Continuous perfusion of ACSF with 0 μM (◦, n=5), 1 μM (▾, n=3), 5 μM (▴, n=5), 10 μM (◆, n=6) or 20 M MeHg (•, n=4) were compared in **A**, the EGL, **B**, the ML, and **C**, the IGL. Significant differences are indicated from untreated control (*) and between 20 μM and 10 μM treatments (#) at the same time point. Intensity values are expressed in arbitrary units (mean ± SEM).

Figure 4. Cell density per $(100\ \mu m)^2$ for CGCs monitored for fluo4 fluorescence intensity, in each layer (EGL, ML and IGL), for tissue treated with different concentrations of MeHg. Fluorescent CGCs were more dense in the EGL and IGL layers than in the ML. At higher MeHg concentrations, fluorescent CGCs in the EGL were more dense than in IGL, but at lower concentrations, density was higher in the IGL. Within the EGL, fluorescent cell density increased significantly with greater concentrations of continuous MeHg treatment, non-overlapping letters are significantly different comparisons ($P<0.05$) Paired comparisons were made between each concentration of MeHg by layer. Significantly different pairs within each layer are indicated by different letters ($P<0.05$). *N* for each treatment is the same as in Figure 3.

Figure 5. Fluorescent cell loss "extinguished" counts from slices during treatment with several concentrations of MeHg over 30 min. Cells extinguished when they lost significant fluo4 fluorescence between time points. Fluo4 fluorescence loss was occasionally associated with visible lysis of cells, so presumably all fluorescence loss is associated with cell death.

Comparisons were made between each concentration of MeHg and untreated control, no comparisons were significantly different ($P>0.05$).

Figure 6. Effect of bicuculline and MeHg on relative fluo4 fluorescence intensity (F/F_0) of CGCs by histological layer. Untreated controls (◦, n=5) and 20 M MeHg alone (•, n=5) are the same as in Figure 3. Bicuculline pulses (arrows, 10 M) with 20 μM MeHg (■, n=4) were compared to bicuculline alone (□, n=3) and MeHg alone. Significant difference are indicated from bicuculline control (*) and from MeHg alone (#) at that time point, $P<0.05$. Intensity values are expressed in arbitrary units (mean ± SEM).

Figure 7. Cell density (per $(100\ \mu m)^2$) for CGCs monitored for fluo4 fluorescence intensity, in each layer (EGL, ML and IGL) and density for the total tissue, for tissue treated with or without MeHg (20 μM) and with or without bicuculline (10 μM). CGCs were more densely distributed in the EGL and IGL layers than in the ML. Paired comparisons were made between MeHg-treated and untreated for each layer. Significantly different pairs within each layer are indicated by different letters ($P<0.05$) Values are mean ± SEM, for the same *n* as described in Figure 6.

Figure 8. Percentage of "extinguished" cells in experiments comparing MeHg and bicuculline treatment. Comparisons were made between 20 and 0 μM MeHg treatments, between bicuculline alone and 0 μM MeHg, between bicuculline alone and bicuculline combined with 20 μM MeHg, and between bicuculline combined with MeHg or MeHg alone. Values are mean ± SEM, for the

JPET Fast Forward. Published on October 29, 2015 as DOI: 10.1124/jpet.115.226761
This article has not been copyedited and formatted. The final version may differ from this version.

same *n* as described in Figure 6.

Figure 9. Effect of muscimol and MeHg on relative fluo4 fluorescence intensity (F/F_0) of CGCs by histological layer. Untreated controls (◦, n=5) and 20 M MeHg alone (•, n=5) are the same as in Figure 3. Muscimol pulses (arrows, 100 M) with 20 μM MeHg (■, n=4) were compared to muscimol alone (□, n=3) and MeHg alone. Significant difference are indicated from muscimol control (*) and from MeHg alone (#) at that time point, $P<0.05$. Intensity values are expressed in arbitrary units.

Figure 10. Cell density (per 100 μm^2) for CGCs monitored for fluo4 fluorescence intensity, in each layer (EGL, ML and IGL) and density for the total tissue, for tissue treated with 20 μM MeHg or untreated and with muscimol (100 μM) or without. CGCs were more densely distributed in the EGL and IGL layers than in the ML. Paired comparisons were made between each concentration of MeHg by layer. Significantly different pairs within each layer are indicated by different letters ($P<0.05$). Values are mean ± SEM with *n* the same as described in Figure 9.

Figure 11. Percentage of "extinguished" cells in experiments comparing MeHg and muscimol treatment. Comparisons were made between 20 and 0 μM MeHg treatments, between muscimol alone and 0 μM MeHg, between muscimol alone and muscimol combined with 20 μM MeHg, and between muscimol combined with MeHg and 20 μM alone. Significantly different pairs within each layer are indicated by non-overlapping letters ($P<0.05$) Values are mean ± SEM with *n* the same as described in Fig. 9.

Fig 1

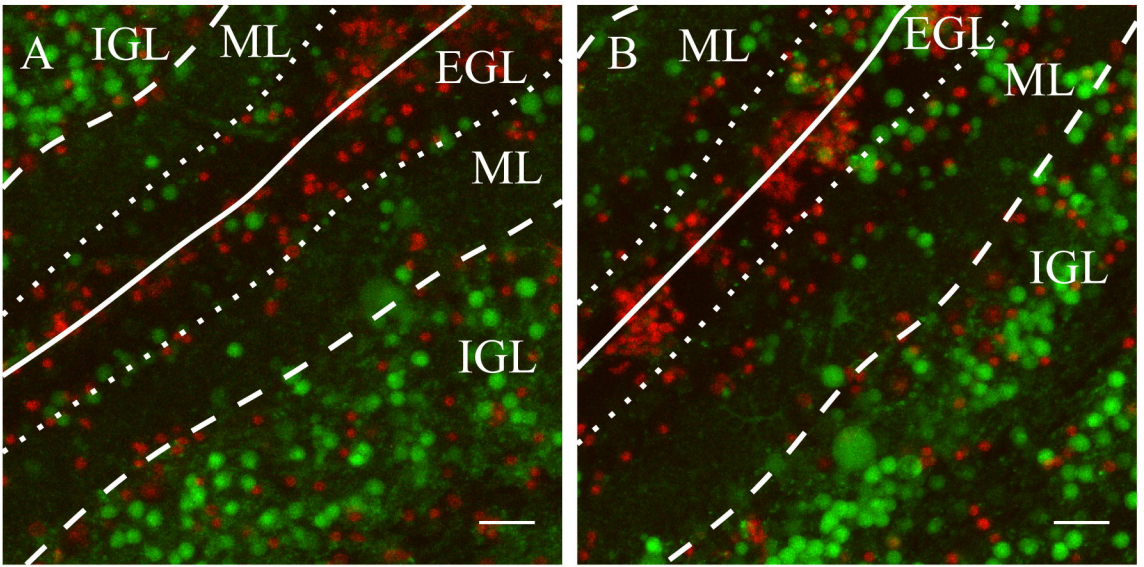
A
IGL
ML
EGL
ML
IGL
B
ML
EGL
ML
IGL

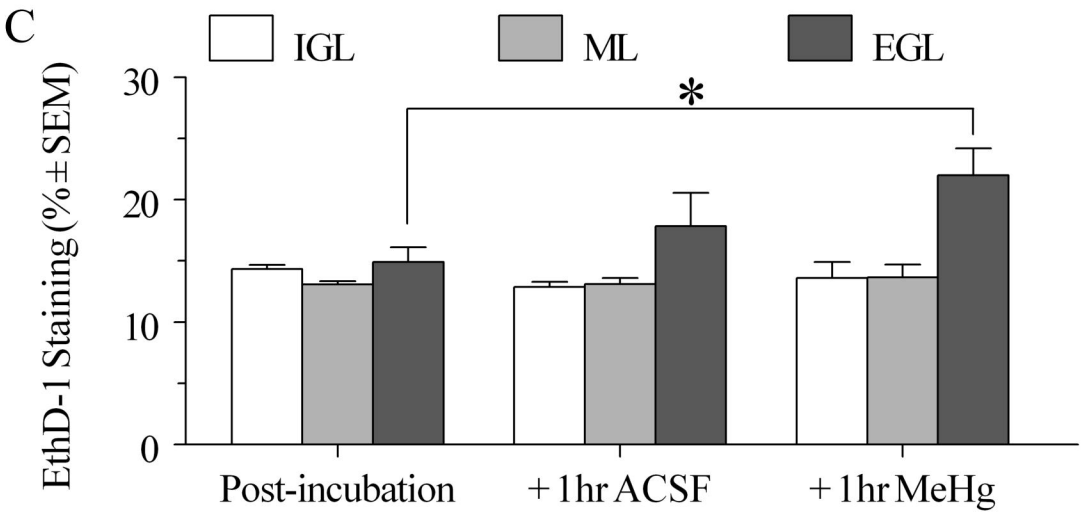
C
IGL
ML
EGL
*
EthD-1 Staining (% ± SEM)
30
20
10
0
Post-incubation
+1hr ACSF
+1hr MeHg

JPET Fast Forward. Published on October 29, 2015 as DOI: 10.1124/jpet.115.226761
This article has not been copyedited and formatted. The final version may differ from this version.

Fig 2

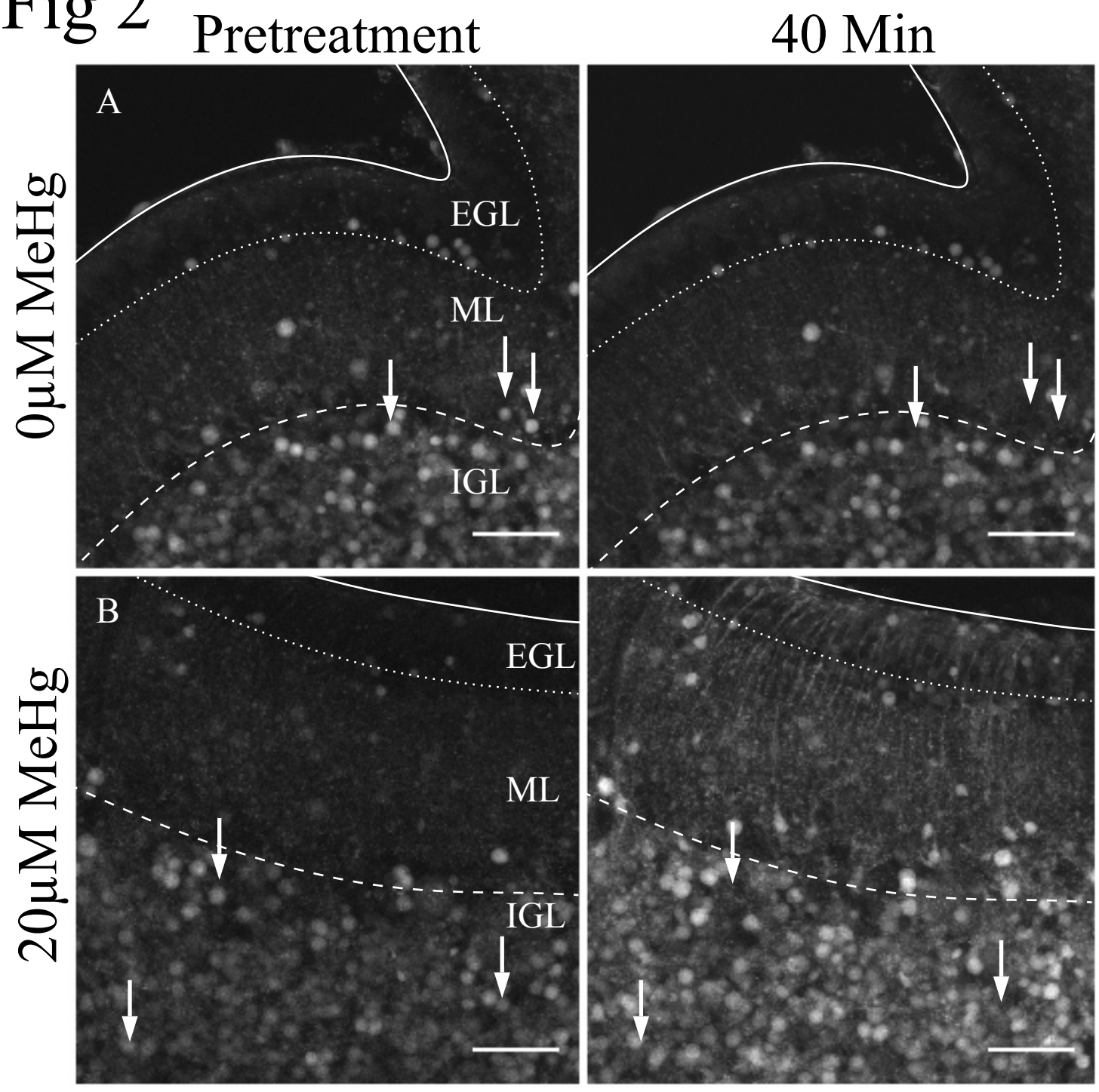

Fig 3

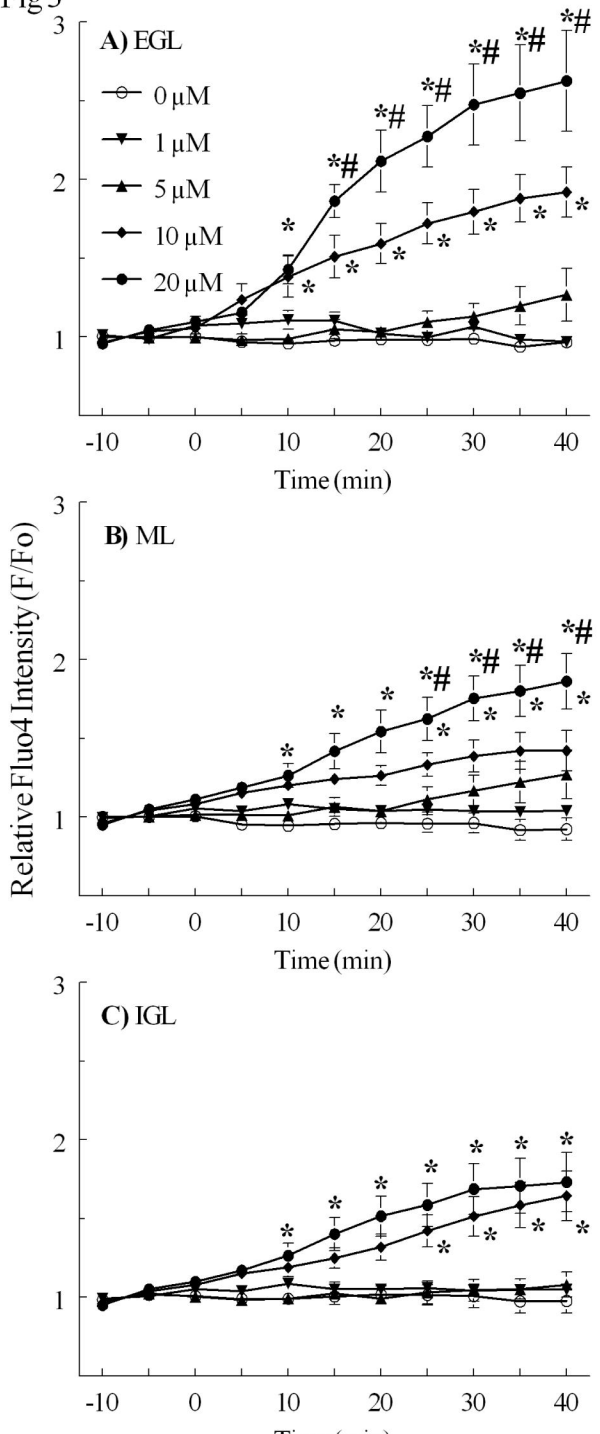
A) EGL
0 μM
1 μM
5 μM
10 μM
20 μM
B) ML
C) IGL
Relative Fluo4 Intensity (F/Fo)
Time (min)
-10
0
10
20
30
40
1
2
3
*
*#

Fig 4

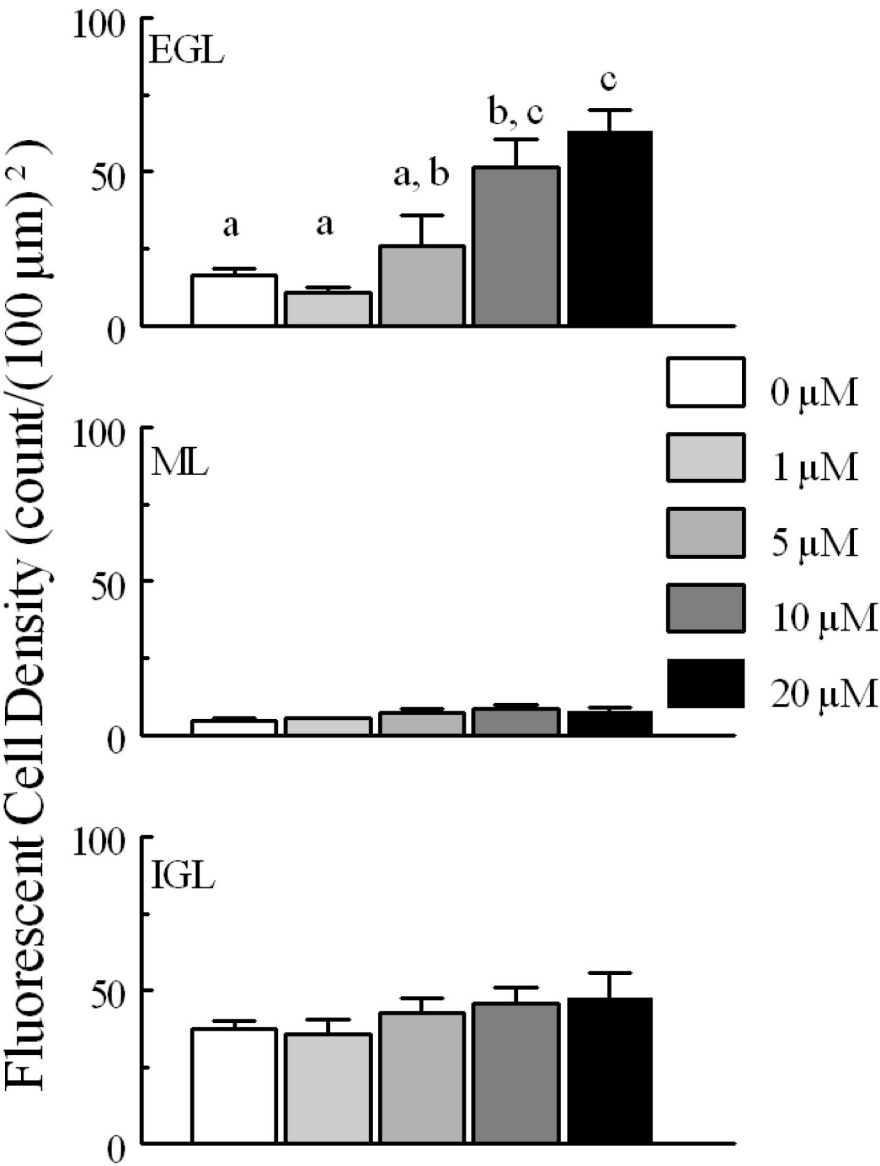
Fluorescent Cell Density (count/(100 μm)²)
EGL
ML
IGL
100
50
0
a
a
a, b
b, c
c
0 μM
1 μM
5 μM
10 μM
20 μM

Fig 5

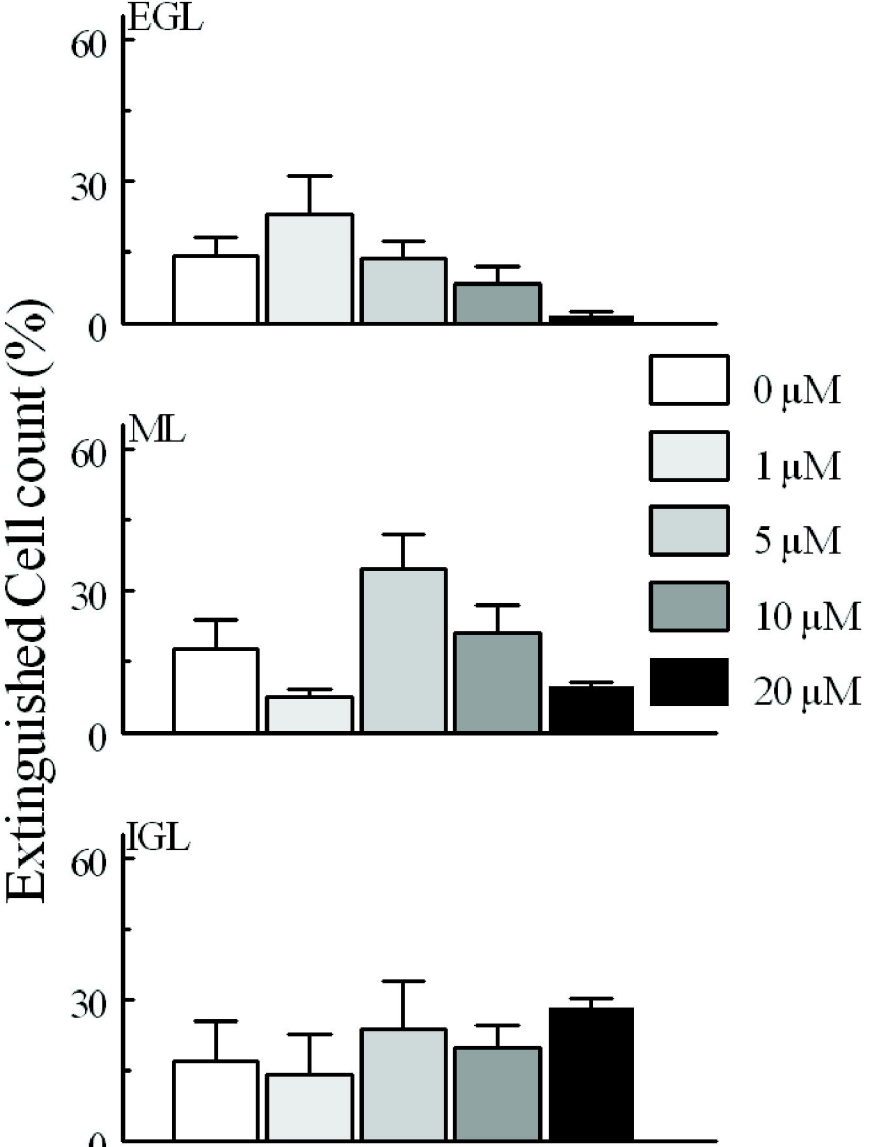
EGL
60
30
0
ML
60
30
0
IGL
60
30
0
Extinguished Cell count (%)
0 μM
1 μM
5 μM
10 μM
20 μM

Fig 6

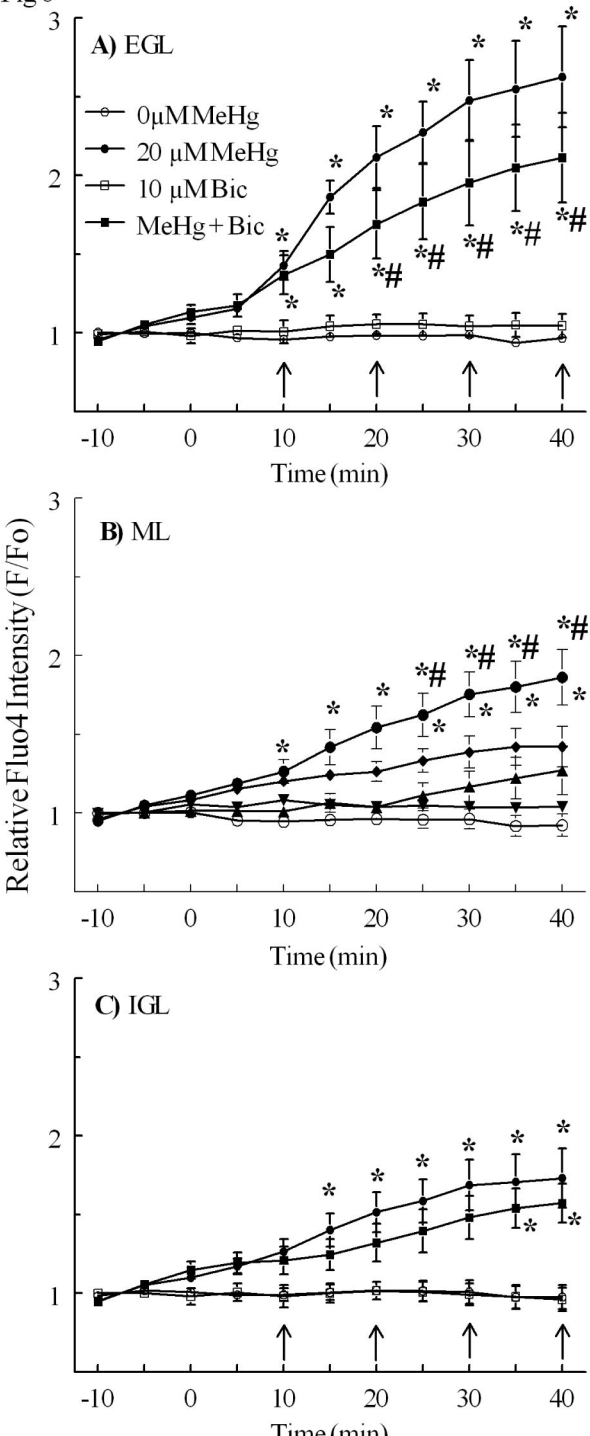
A) EGL
0μMMeHg
20 μMMeHg
10 μMBic
MeHg+Bic
B) ML
C) IGL
Relative Fluo4 Intensity (F/Fo)
Time (min)
-10
0
10
20
30
40
1
2
3

Fig 7

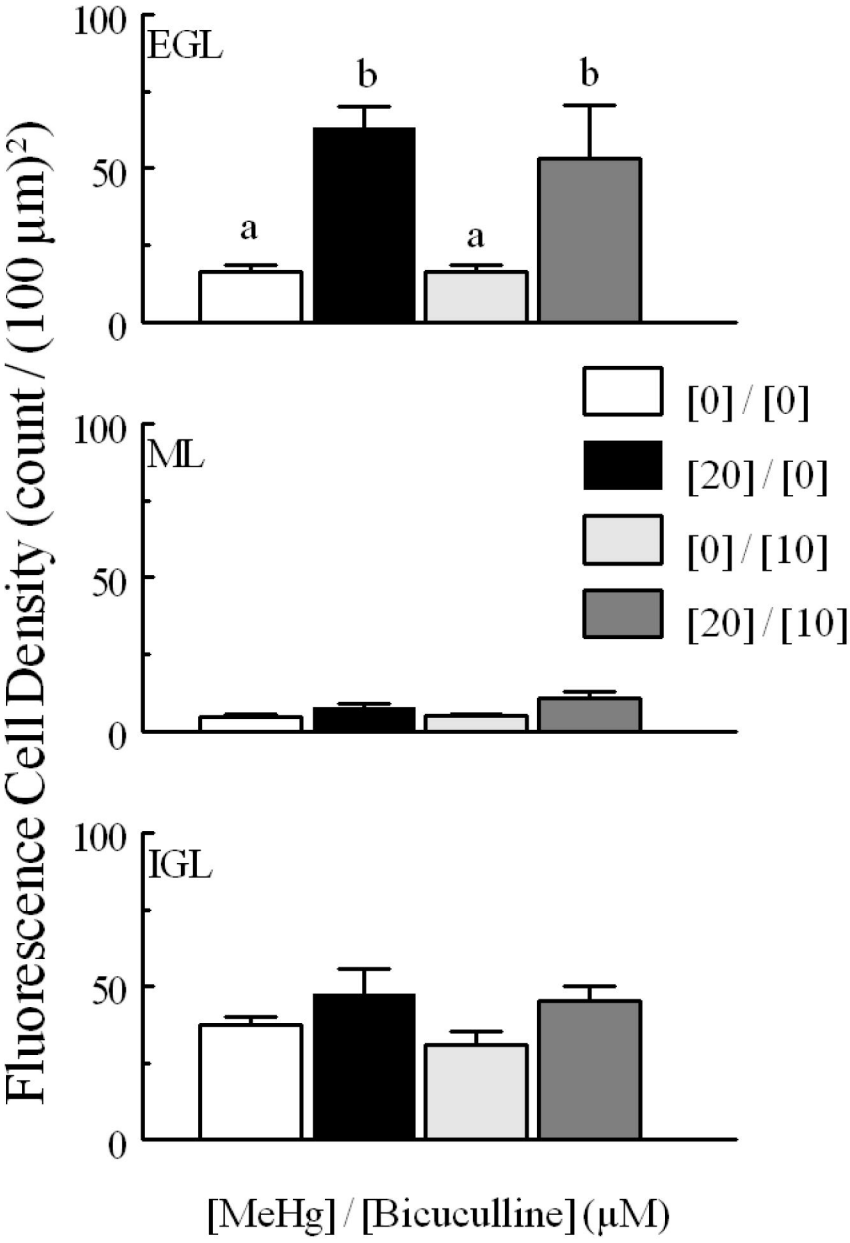
EGL
ML
IGL
100
50
0
a
b
a
b
[0] / [0]
[20] / [0]
[0] / [10]
[20] / [10]
Fluorescence Cell Density (count / (100 μm)²)
[MeHg] / [Bicuculline] (μM)

Fig 8

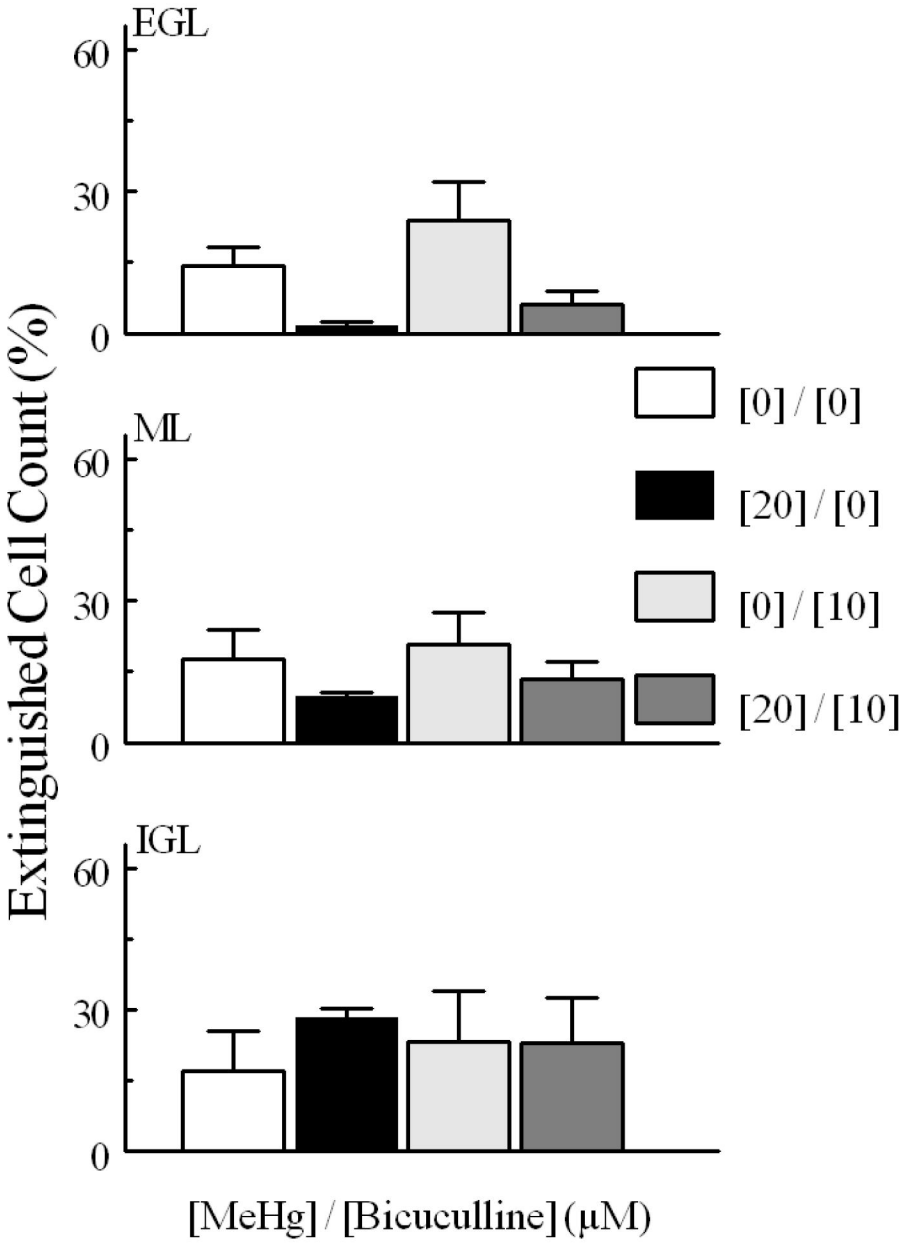
EGL
60
30
0
ML
60
30
0
IGL
60
30
0
Extinguished Cell Count (%)
[0] / [0]
[20] / [0]
[0] / [10]
[20] / [10]
[MeHg] / [Bicuculline] (μM)

Fig 9

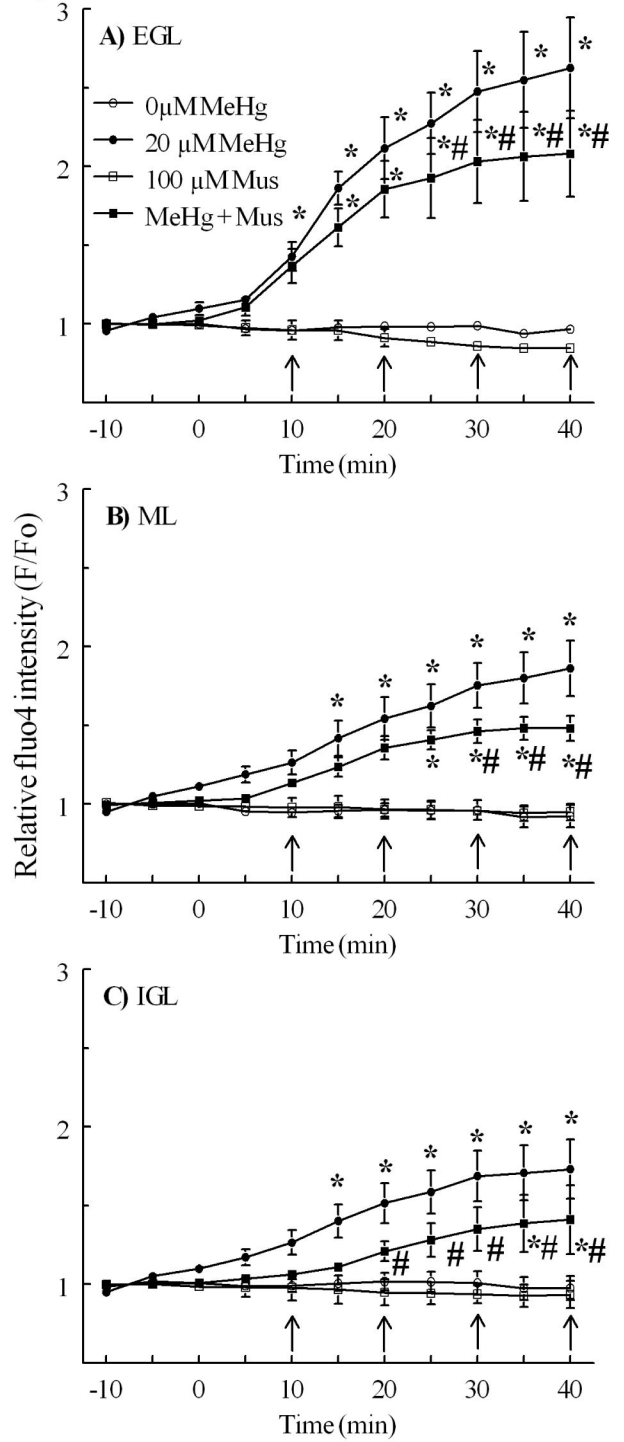
A) EGL
0μMMeHg
20 μMMeHg
100 μMMus
MeHg+Mus
B) ML
C) IGL
Relative fluo4 intensity (F/Fo)
Time (min)
-10
0
10
20
30
40
1
2
3

Fig 10

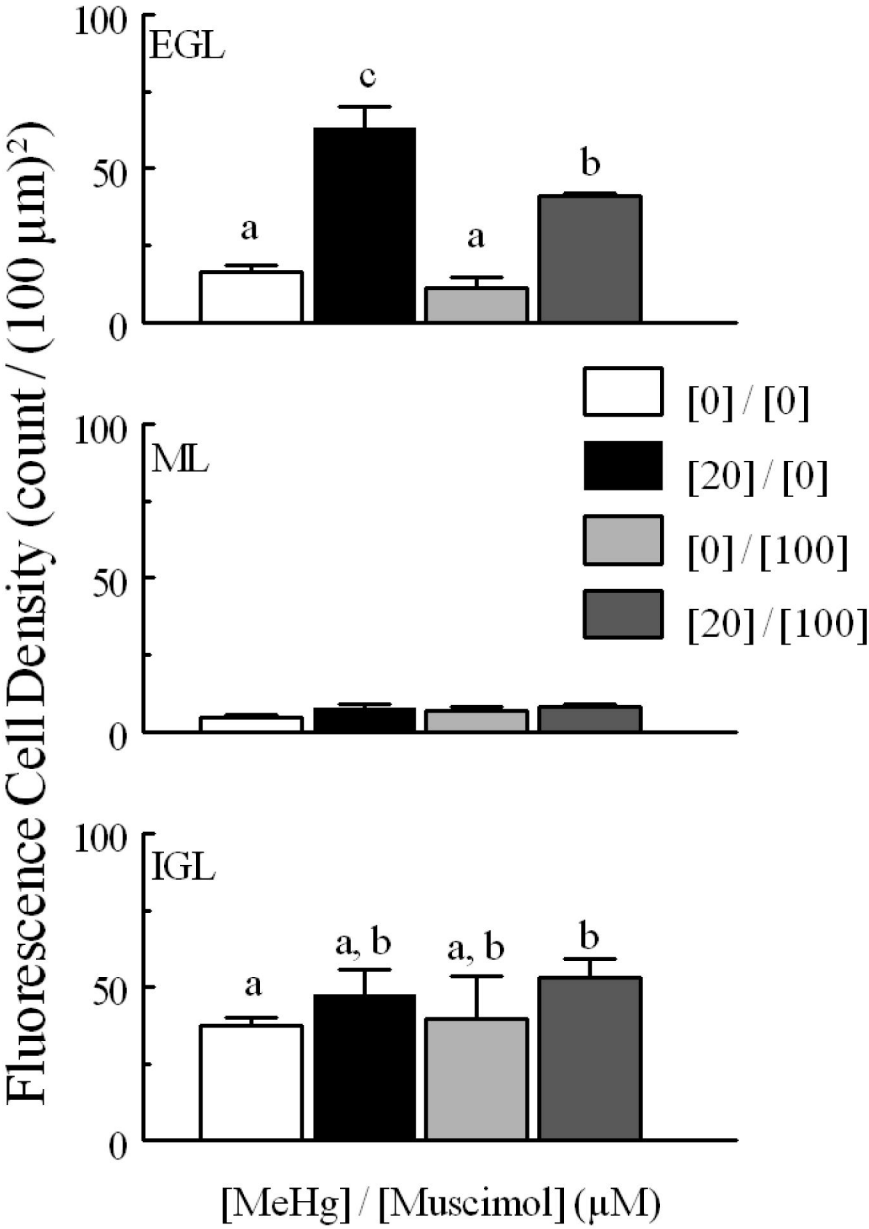
EGL
ML
IGL
100
50
0
a
c
a
b
a, b
a, b
b
[0] / [0]
[20] / [0]
[0] / [100]
[20] / [100]
Fluorescence Cell Density (count / (100 μm)²)
[MeHg] / [Muscimol] (μM)

Fig 11

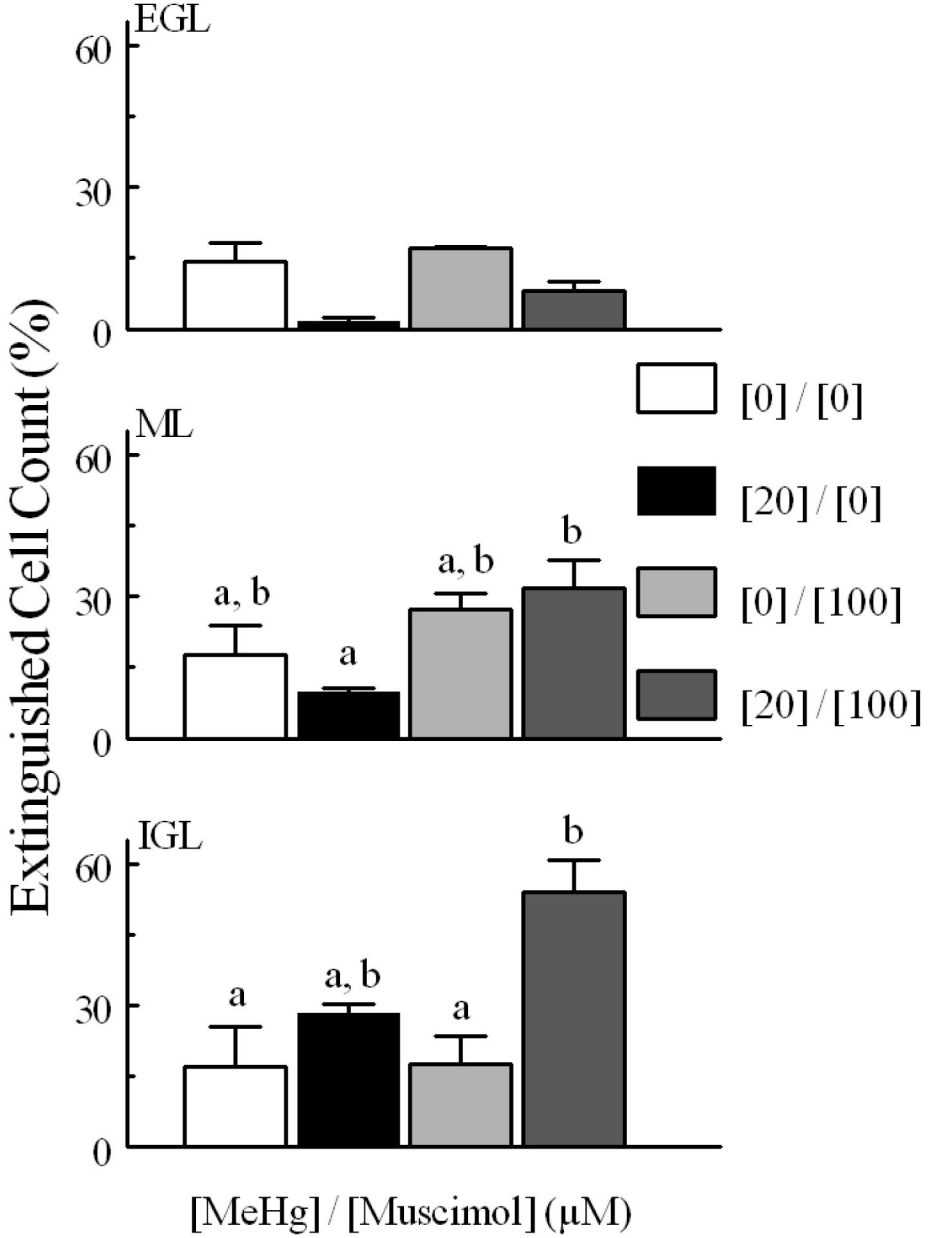
EGL
ML
IGL
60
30
0
Extinguished Cell Count (%)
a, b
a
a, b
b
a
a, b
a
b
[0] / [0]
[20] / [0]
[0] / [100]
[20] / [100]
[MeHg] / [Muscimol] (μM)